



The nature of 6,6'-bis(triphenylamine) substituted BINOL as chromophoric and fluorogenic hybrid chemosensor for selective fluoride detection

Chi-Hsiang Chen, Man-kit Leung*

Department of Chemistry and Institute of Polymer Science and Engineering, National Taiwan University, 1, Roosevelt Road Section 4, Taipei 106, Taiwan, ROC

ARTICLE INFO

Article history:

Received 3 December 2010

Received in revised form 12 March 2011

Accepted 17 March 2011

Available online 25 March 2011

Keywords:

BINOL

Anion recognition

Hydrogen bond complexation

Chromophoric and Fluorogenic sensor

Triphenylamine

ABSTRACT

6,6'-Bis(triphenylamine)-1,1'-binaphthyl-2,2'-diol (**1**) is highly fluorescent in visible region. On treatment with a variety of anions, the UV–vis absorption as well as the fluorescent behavior of **1** in CH₂Cl₂ is substantially changed. Among the tetrabutylammonium (TBA) salts we tested, including F⁻, OH⁻ (from TBAOH in MeOH), Cl⁻, Br⁻, I⁻, OAc⁻, HSO₄⁻, TsO⁻ (Et₄N salt), and H₂PO₄⁻, F⁻ was found to be the most effective fluorescence quencher. Quantitative fluorescence analysis of the titration data revealed that the anions are classified into two categories: (1) Simple mono-anions, such as F⁻ (log β₂^F = 11.00 ± 0.08), OH⁻ (log β₂^{OH} = 9.05 ± 0.01), and Cl⁻ (log β₂ = 9.96 ± 0.70) that follow the stoichiometry of 1:2, indicating the formation of (1·X₂)²⁻ complexes; (2) Oxo-anions, such as OAc⁻ (log β₁^{OAc} = 5.13 ± 0.012), H₂PO₄⁻ (log β₁^{HP} = 4.87 ± 0.03), and TsO⁻ (using tetraethylammonium salt, (log β₁^{OTs} = 3.36 ± 0.02) that show the stoichiometry of 1:1, indicating the formation of (1·X)⁻ complexes. The complexation behaviors were further confirmed by ¹H NMR spectroscopy. In the co-crystal prepared from 1,1'-binaphthyl-2,2'-diol (BINOL) and Et₄NF, F⁻ and BINOL are assembled to form a linear polymeric array, with a dimeric group of BINOL/BINOL anions linked as the side-chains. Intramolecular hydrogen bond was observed within the BINOL anion. This provides structural insights about the BINOL–fluoride complex formation.

© 2011 Elsevier Ltd. All rights reserved.

1. Introduction

Miniaturizing optoelectronic devices into nanometer-scale is one of the major challenges for modern technologies.^{1–3} Supramolecular chemistry may provide the ultimate solution to solve these problems. There are many advantages of using supramolecules due to their well-defined chemical structures and physical properties, high structural stability, availability of mature synthetic technology, as well as their tunable photo-physical and electronic properties.^{4–7} Many research teams have reported the design of supramolecular sensors,^{8–12} utilizing the mechanism of photochemical isomerization,¹³ redox reactions,¹⁴ or acid–base interactions,^{15–22} in which molecular recognition plays important roles on their designs. In addition, to establish useful electronic array for detection, those recognition systems have to be robust so that they can tolerate harsh conditions under photochemical or electrochemical environments.^{23,24}

Detection of fluoride ion has attracted a lot of attention during the last couple of decades.^{25,26} Designs based on the specific Lewis acid–base interaction, such as the strong binding of boron atom with fluoride ion have been reported.^{27–38} Furthermore, sensors based on the hydrogen-bonding system, such as urea,^{39–48} thiourea,^{49–52}

amide,^{53–55} imidazole,^{56–59} pyrrole,^{60–62} acridinium,⁶³ and phenol and their corresponding silyl ether^{64–74} have also been developed.

1,1'-Bi-2-naphthol (BINOL) is a commercially available material that can be synthesized and functionalized in large quantity. In addition, the outstanding C₂ chiral properties make BINOL a famous ligand for asymmetric synthesis^{75–77} as well as a chiral induction core for sensors.^{78–81} Although in principle two proximate phenolic protons on BINOL would provide perfect binding-environment for anions, examples about the use of BINOL for sensing anions are rare. This is probably due to the lack of: (1) chromophores to show photo-physical response in the visible region and (2) fluorophores that show high quantum efficiency. Nevertheless, some studies have been reported during the last decade. For examples, Iwanek and Mattay, Wang, and Pu have independently reported the application of fluorescence recognition of BINOL for amines,⁸² amino-alcohols,⁸³ and mandelic acid^{84–86} detection. Kumar and Yu have, respectively, reported the use of 3,3'-disubstituted BINOL derivative to facilitate fluoride ions detection.^{87,88} Ito has evaluated the BINOL anion recognition using ¹H NMR spectroscopy.⁸⁹ On the other hand, Shinmyozu has reported the study of *stiff*-stilbene connected bis-BINOL and its binding behavior with anions.⁹⁰ Crystal structures of BINOL-monoalkyltrimethylammonium halides co-crystals have been reported by Marfo-Owusu.⁹¹

Herein we report a rational design and the nature of **1** for anion recognition, in particular on fluoride sensing (Fig. 1). In our design,

* Corresponding author. E-mail address: mkleung@ntu.edu.tw (M.-kit Leung).

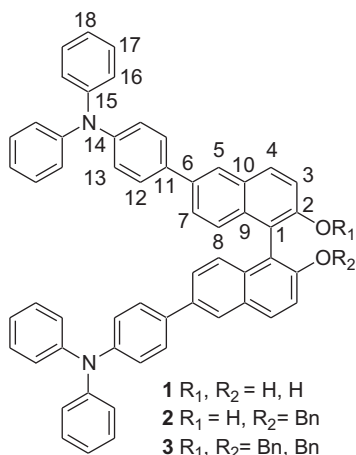


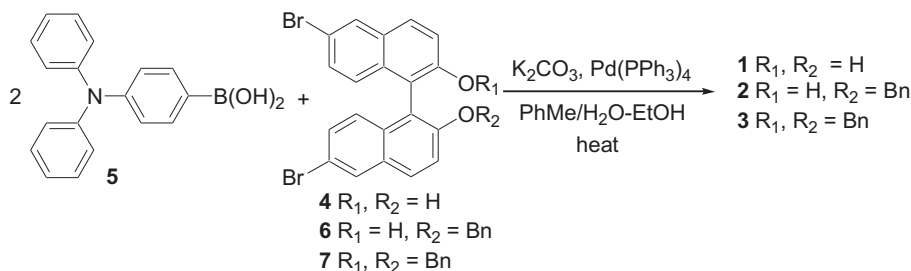
Fig. 1. Chemical structures of 1–3.

the conjugative π -system on the BINOL subunit has been modified by introducing two electron-rich $\text{Ph}_2\text{NC}_6\text{H}_4$ -groups at the 6,6'-positions that shows different binding behavior from the 3-substituted and 3,3'-disubstituted BINOLs. The corresponding absorption and emission λ_{max} 's are extended to the visible region so that the sensory response could be visually detected. When **1** binds with anions, the π -conjugation systems of **1** would be perturbed, leading to a change of the spectral response. In the present work, compounds **1**–**3** were prepared and their binding behaviors were discussed.

2. Results and discussion

2.1. Synthesis

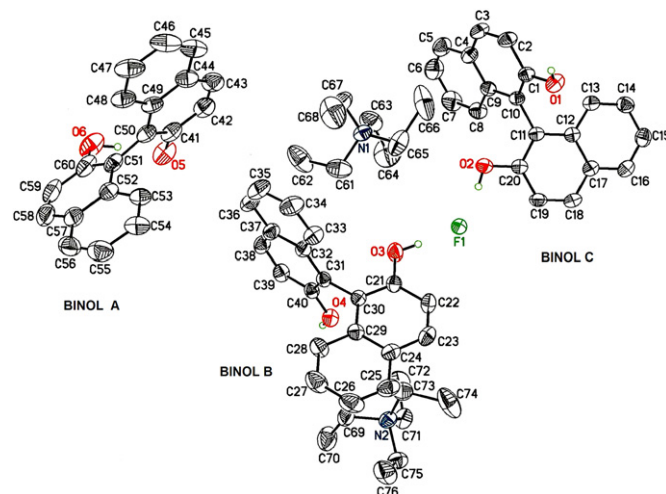
Compounds **1** was prepared from condensation of 6,6'-dibromo-1,1'-binaphthyl-2,2'-diol⁹² (**4**) with the corresponding boronic acid **5**⁹³, using the Suzuki coupling conditions of $\text{Pd}(\text{PPh}_3)_4/\text{K}_2\text{CO}_3/\text{PhCH}_3\text{--H}_2\text{O--EtOH}$ as catalyst (Scheme 1). In addition, dibromide **4** could also be either mono- or di-benzylated to give **6** and **7**, followed by Suzuki coupling⁹⁴ with **5** to give **2** and **3**, respectively.



Scheme 1. Synthetic pathways for 1–3.

2.2. Crystallographic analysis

2.2.1. The structure of the co-crystal from binaphthyl-2,2'-diol (BINOL) and Et_4NF . The tendency of BINOLs to form complexes with fluoride ions in the solid state was first examined by X-ray studies. On slow evaporation of a saturated solution containing 2 M equiv of Et_4NF and 1 M equiv of BINOL in CH_2Cl_2 , co-crystals of a salt of formula $[\text{Et}_4\text{N}^+]_2[\text{F}^-][\text{BINOL}]_2[\text{BINOL anion}]$ were obtained. The ORTEP diagram of the co-crystal is shown in Fig. 2. Three BINOL units, denoted as BINOL A, BINOL B, and BINOL C, are contained in the

Fig. 2. ORTEP of the co-crystal of $[\text{Et}_4\text{N}^+]_2[\text{F}^-][\text{BINOL}]_2[\text{BINOL anion}]$.

crystal lattice, in which the hydrogen bond interactions between F^- and BINOL were found. A simplified sketch is shown in Fig. 3. First of all, F^- binds with BINOL B through hydrogen bond interactions to form linear arrays. Secondly, intramolecular hydrogen bond occurs between the oxygen atoms of the anionic BINOL A. In addition, the anionic BINOL A and BINOL C are bound to a dimeric group through intermolecular hydrogen bond interactions.

While the bond lengths of $\text{O}(1)\text{--C}(1)$ (1.355 (3) Å), $\text{O}(2)\text{--C}(20)$ (1.356 (3) Å), $\text{O}(3)\text{--C}(21)$ (1.349 (3) Å), $\text{O}(4)\text{--C}(40)$ (1.352 (3) Å), and $\text{O}(6)\text{--C}(60)$ (1.356 (3) Å) are almost identical, the bond length of $\text{O}(5)\text{--C}(41)$ (1.312 (3) Å) on BINOL A is particularly short, indicating that $\text{O}(5)$ is deprotonated. The dihedral angle of $54.1 (3)^\circ$ between the naphthyl rings on BINOL A is much smaller in comparison to that of $85.8 (3)^\circ$ and $106.6 (2)^\circ$ for the BINOLs B and C, indicating that the geometry of the BINOL anion is relatively flat. The observation of the flat geometry suggested that the charge-delocalization between two naphthyl rings of BINOL A is important. The short distance of 2.533 Å between $\text{O}(5)$ and $\text{O}(6)$ illustrates the existence of the intramolecular hydrogen bond. In addition, intermolecular hydrogen

bond between BINOL A and BINOL C is evidenced on the basis of the short distance of 2.594 Å between $\text{O}(5)$ and $\text{O}(1)$.

The simplified sketched clearly illustrated that the fluoride ions and the BINOL B molecules, colored in green, are assembled to form a linear polymeric structure, with dimeric pair of BINOL C/BINOL A anion, colored in yellow, linked as the side-chains. This provides structural insights about the BINOL-fluoride complex formation. Each F^- is surrounded by three --OH groups in the lattice. The distances of 2.560 Å for $\text{F}(1)\text{--O}(2)$, 2.547 Å for $\text{F}(1)\text{--O}(3)$, and 2.515 Å for the $\text{F}(1)\text{--O}(4)$ of the adjacent BINOL units were

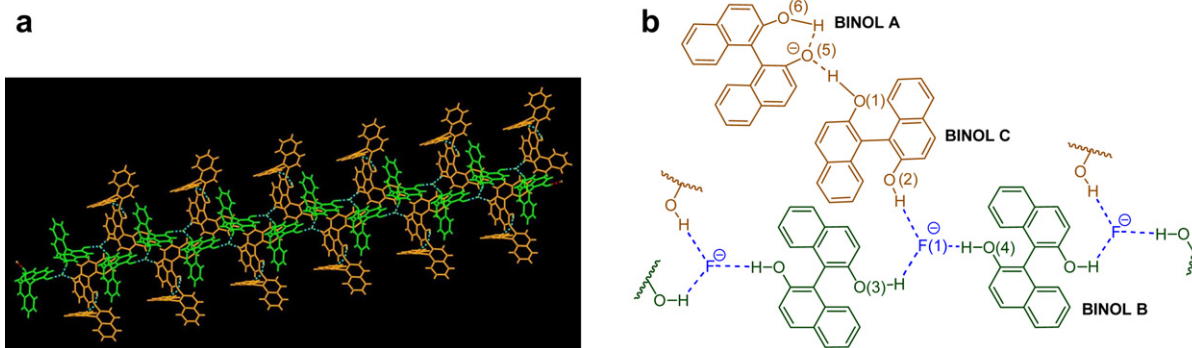


Fig. 3. The linear polymeric structure in the crystal lattice of $[\text{Et}_4\text{N}^+]_2[\text{F}^-][\text{BINOL}]_2[\text{BINOL anion}]$: (a) A simplified sketch of the polymeric linear-array. The Et_4N^+ counter ions were omitted in order to simplify the sketch. (b) The schematic diagram that shows the connectivity between all components.

measured. The short O–F distances indicate that the hydrogen bonding interactions are strong.

2.3. UV–vis spectrophotometric studies

2.3.1. The interaction on **1 with anions in organic solvents, studied by UV–vis absorption spectrophotometry.** Compound **1** exhibits a major absorption band centered at 340 nm with a shoulder band at around 300 nm (Fig. 4). The spectral change in various solvents, including hexane ($\lambda_{\text{max}}=338$ nm), PhMe ($\lambda_{\text{max}}=341$ nm), CH_2Cl_2 ($\lambda_{\text{max}}=340$ nm), and CH_3CN ($\lambda_{\text{max}}=336$ nm), is small, indicating that photo-induced charge transfer (CT) absorption in the ground state is insignificant. The PM5-ZINDO-s calculations⁹⁵ revealed that the absorption band at 340 nm is constituted of two electronic transitions: (a) the local excitation of the triphenylamine group; (b) the CT transitions from the triphenylamine group to the BINOL subunit. The local electronic transition energies of the triphenylamine core are slightly lower than that of the CT transitions. The local $\pi-\pi^*$ transitions of the BINOL subunit, on the other hand, contribute to the band at 300 nm.

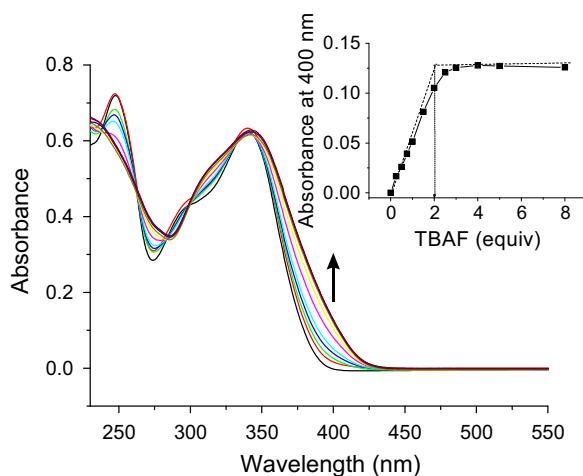


Fig. 4. Spectral changes of **1** (1×10^{-5} M) during fluoride titration: the molar equivalents of TBAF were: 0, 0.25, 0.50, 0.75, 1.0, 1.5, 2.0, 2.5, 3.0, 4.0, 5.0, and 8.0. In the inset is shown a plot of the absorbance growth at 400 nm versus the molar equivalents of TBAF.

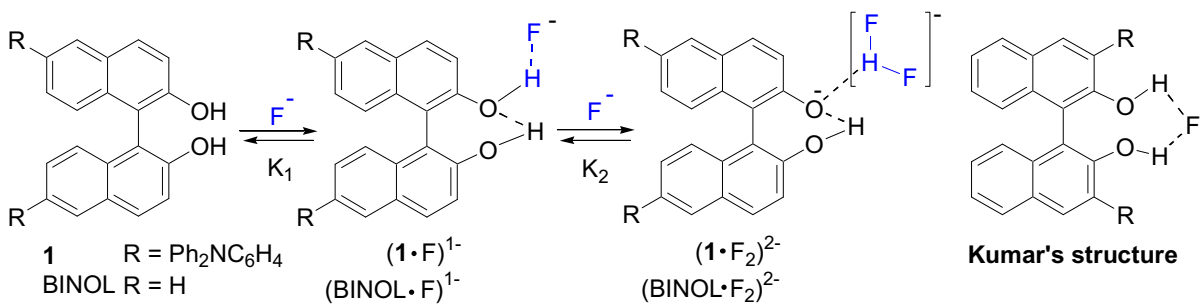
2.3.2. Spectrophotometric titration in CH_2Cl_2 . While addition of excess amounts of tetrabutylammonium (TBA) salts of Cl^- , Br^- , I^- , and HSO_4^- to **1** does not induce any significant spectral changes, addition of F^- , OH^- , acetate (OAc^-), tosylate (OTs^-), and H_2PO_4^- induces a new red-shifted shoulder band at around 400 nm. Fig. 4 shows the traces of the UV–vis spectral changes of **1** (1×10^{-5} M) during the titration with

F^- . The lack of the well-defined spectral isobestic point suggested that multi-step equilibria are involved in the complexation process. Inset in Fig. 4 shows the plot of the absorbance change at 400 nm versus the molar equivalents of TBAF used in the titration. The absorbance gradually arises and reaches to a plateau at the 2-equiv point, indicating a model of strong binding for $(\mathbf{1} \cdot \text{F}_2)^{2-}$ complex formation.

Similar stepwise changes in F^- titration have been reported in other hydrogen-bonding system, such as urea-fluoride interactions.^{39–48} In those cases, the first added F^- would establish hydrogen bond with the urea protons while the second added F^- would have the weakly acidic urea protons abstracted to form HF_2^- . With regard to the weak acidity of the BINOL protons ($\text{p}K_a=10$)⁷⁷, it is reasonable to propose similar mechanisms in the present case. An expression for the entire process of fluoride complexation is depicted in Scheme 2, in which K_1^{F} and K_2^{F} are the equilibrium constants of each step and $\beta_2=K_1^{\text{F}} \cdot K_2^{\text{F}}$ is defined as the overall complex formation constant. The first step involves hydrogen bond formation to give $(\mathbf{1} \cdot \text{F})^-$ that usually causes minimal perturbations on the π -chromophore. The structure of $(\mathbf{1} \cdot \text{F})^-$ being proposed here is based on the structure of the anionic BINOLA, which is further hydrogen bonded to another hydrogen bond donor in the co-crystal. However, the structure proposed by Kumar^{20a} is another reasonable option for $(\mathbf{1} \cdot \text{F})^-$ that cannot be excluded. The weak interaction might not lead to significant change in the absorption spectrum. However, proton transfer should take place in the presence of the second F^- to form $(\mathbf{1} \cdot \text{F}_2)^{2-}$. It has been known that more basic the acceptor and stronger the hydrogen bond accepting ability, the more advanced the proton transfer would be. HF_2^- is the most-stable hydrogen bond complex that fluoride can form in $(\mathbf{1} \cdot \text{F}_2)^{2-}$. With more the negative charge localized on the oxygen atoms, more monoanion-like the BINOL would behave. A shoulder of the charge-transfer absorption could therefore be observed at 400 nm. Since one might concern that the free anion may also give rise to similar absorption, we have further examined for other anions with different basicity and discovered that addition on OAc^- , H_2PO_4^- , and OTs^- would also lead to the uprising of the red-shifted band. Since OTs^- is considered as a relatively weak base, deprotonation of **1** with OTs^- to form free $\mathbf{1}^-$ is unlikely, indicating that the UV absorption at around 400 nm is presumably arising from the hydrogen bond complex formation.

To doubly confirm the origin of the red-shifted band, titration had been carried out for BINOL with TBAF. Upon addition of F^- , the band at 375 nm progressively develops and reaches to a plateau at the 2-equiv point. All these again evidence that the BINOL rather than the triphenylamine subunit is crucial for the complexation and corresponds to the spectral change.

Compound **1** also gives rise to the spectral change when being titrated with H_2PO_4^- . However, the stoichiometry was found to be different. Although similar spectral changes at 400 nm were observed, the different stoichiometry of 1:1 with $\log \beta_1^{\text{HP}} = 4.36 \pm 0.01$ was



found. The binding model was established on the basis of the linear-plot of $A_i/(A_f - A_i)$ versus $[\text{H}_2\text{PO}_4^-]$, in which A_i is the absorbance of the sample at i molar equivalents and A_f is the final limit of absorbance of the sample in the presence of large excess of H_2PO_4^- (Fig. 5). The equations are derived as follows: on the basis of the equilibrium shown in Scheme 3, the formation constant β_1^{HP} is defined.

The value of β_1^{HP} was therefore estimated as the slope in the plot $A_i/(A_f - A_i)$ versus $[\text{H}_2\text{PO}_4^-]$. Although we have no clue about the structure of the $(\mathbf{1}\cdot\text{H}_2\text{PO}_4)^{1-}$ complex, we believed that the H_2PO_4^- would be first hydrogen bonded to one phenolic proton. The dipolar P=O bond might be further hydrogen-bonded to the second phenolic protons, as shown in Scheme 3, through a six-membered

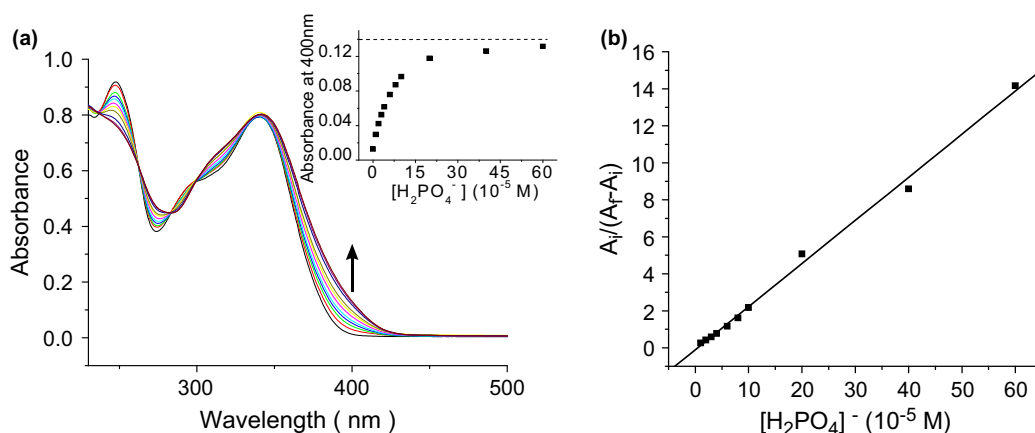
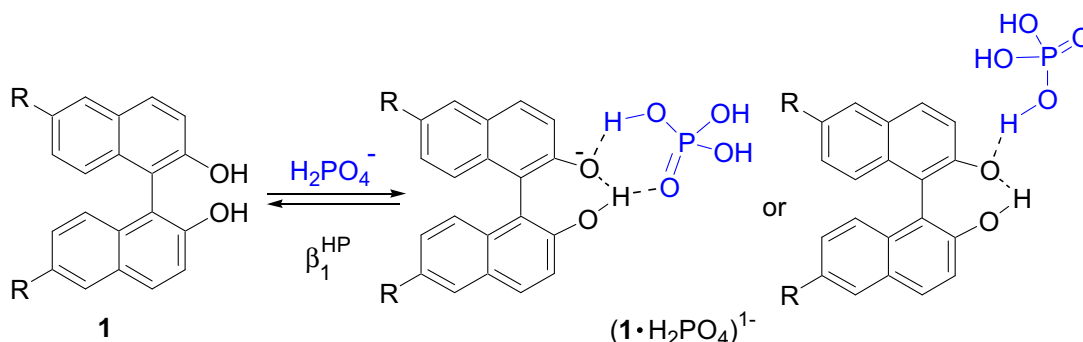


Fig. 5. (a) Spectral changes of **1** (1×10^{-5} M) during H_2PO_4^- titration. The molar equivalents of TBA- H_2PO_4 used were: 0, 1, 2, 3, 4, 6, 8, 10, 20, 40, and 60. In the inset is the plot of the absorbance growth at 400 nm versus $[\text{H}_2\text{PO}_4^-]$ used, with the $A_f = 0.13$ was estimated. (b) A linear-correlation plot of $A_i/(A_f - A_i)$ versus $[\text{H}_2\text{PO}_4^-]$.



$$\beta_1^{\text{HP}} = \frac{[(\mathbf{1}\cdot\text{H}_2\text{PO}_4^-)]}{[\text{H}_2\text{PO}_4^-][\mathbf{1}]}$$

Rearrangement of the above equation leads to the following relationship.

$$[\text{H}_2\text{PO}_4^-] \cdot \beta_1^{\text{HP}} = \frac{[(\mathbf{1}\cdot\text{H}_2\text{PO}_4^-)]}{[\mathbf{1}]} = \frac{A_i}{A_f - A_i}$$

hydrogen bond array to provide a bifurcate structure. In this situation, the hydrogen bond interactions would be strengthened.

2.4. Fluorescence studies

2.4.1. Fluorescence behavior of 1. On the contrary to the small solvent dependency in the absorption spectra, **1** fluoresces at around 400 nm, depending on the solvent system (Fig. 6). The red-shifts span about a range of 46 nm, from 390 nm in hexane to 436 nm in CH_3CN . While vibronic features could be observed in hexane, the

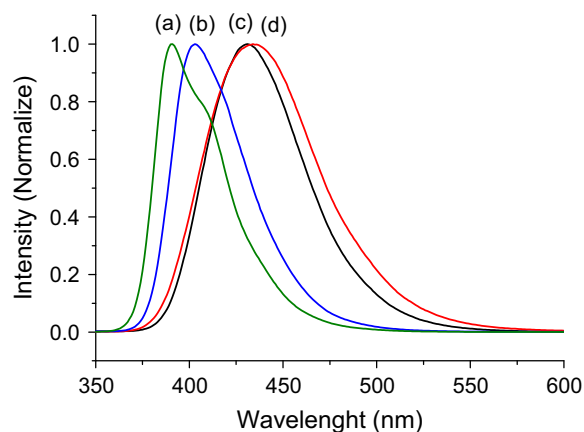


Fig. 6. Emission spectra of **1** in (a) hexane (green with $\lambda_{\text{max}}=390$ nm), (b) toluene (blue, $\lambda_{\text{max}}=403$ nm), (c) CH_2Cl_2 (black, $\lambda_{\text{max}}=430$ nm), and (d) CH_3CN (red, $\lambda_{\text{max}}=436$ nm).

emission spectra become broad in polar solvents. All these suggest that certain extents of structural relaxation along with CT characters are established in the emissive excited state. The CT state may involve electron donation from the electron-rich triphenylamine groups to the BINOL component. Since this polar CT excited state is stabilized in a polar solvent, a reduction of the energy-gap and hence red-shifting of the emission spectra is expected.⁹⁶ However, the essences about the structural relaxation process are still uncertain. In general, photo-excited states can undergo stabilization by geometrical relaxation. Biphenyl is a prominent example that has been reported, in which flattening in the excited state is driven by an increase of mesomeric interactions.^{97–99} However, it has recently reported that in the cases of phenylpyrene derivatives, flattening is the major relaxation pathway in non-polar solvent, whereas in highly polar solvents stabilization of the charge-transfer state by further twisting has been evidenced.^{100,101}

2.4.2. Fluorescence titration with fluoride ions. The binding behavior of **1** (1×10^{-6} M) with F^- in dried CH_2Cl_2 was monitored by fluorescence quenching experiments. As shown in Fig. 7, the fluorescence intensity of **1** was gradually reduced during titration and almost 95% of the signal was quenched after 10 M equiv of TBAF had been introduced. To avoid the self-absorption interference arising from CT band, non-linear curve fitting was performed, using the

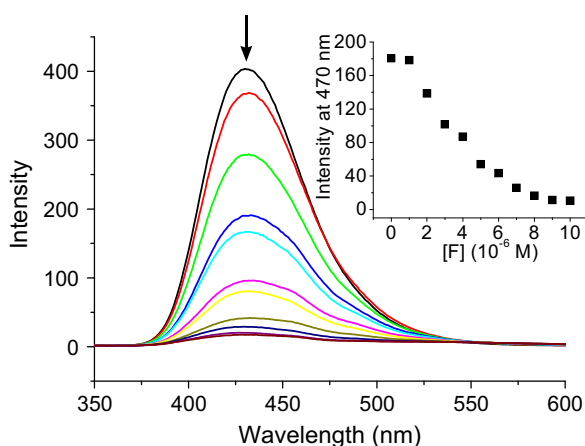


Fig. 7. Quenching of the fluorescence intensity of **1** (1×10^{-6} M) during the titration with F^- . The molar equivalents of TBAF used were: 0, 1, 2, 3, 4, 5, 6, 7, 8, 9, and 10. In the inset is demonstrated a linear-correlation plot between the value of I_0/I_i versus $[\text{F}^-]^2$.

fluorescence intensity I_0 and I_i at 470 nm, and the concentration of $[\text{F}^-]$ into the equation of

$$\frac{I_0 - I_i}{I_i} = \frac{\beta_2^{\text{F}} [\text{F}^-]^2}{1 + K_1^{\text{F}} [\text{F}^-]}$$

The data fitted well to the equation up to 75% of fluorescence quenching, indicating that the binding should follow the 1:2 stoichiometry.¹⁰² The binding constants of $\log \beta_2^{\text{F}} = \log (K_1^{\text{F}} \cdot K_2^{\text{F}}) = 11.00 \pm 0.08$, $\log K_1^{\text{F}} = 4.43 \pm 0.11$, and $\log K_2^{\text{F}} = 6.57 \pm 0.19$ were estimated accordingly. The value of $\log K_1^{\text{F}}$ is in good agreement with that reported by Kumar in their system.⁸⁷ As shown in the inset of Fig. 7, the fluorescence intensity remains almost unchanged during the first molar equivalents of F^- being added, indicating that the CT character on $(\mathbf{1} \cdot \text{F})^-$ is weak. However, when more equivalents of F^- being added, formation of $(\mathbf{1} \cdot \text{F}_2)^{2-}$ would lead to fluorescence quenching. This observation is consistent with the results in UV–vis titrations.

Similar titration behavior with the same stoichiometry of 1:2 was also observed for using TBAOH in MeOH as the base. The binding constants of $\log \beta_2^{\text{OH}} = \log (K_1^{\text{OH}} \cdot K_2^{\text{OH}}) = 9.05 \pm 0.01$, $\log K_1^{\text{OH}} = 3.86 \pm 0.42$, and $\log K_2^{\text{OH}} = 5.19 \pm 0.43$, were measured. In these experiments, the commercially available TBAOH in MeOH (0.1 M) was used as the titrant. It has to be noted that perhaps due to the interactions with MeOH molecules, the activity of TBAOH is not as strong as we expected; the binding ability of OH^- to **1** was found to be slightly weaker than that of F^- . Nevertheless, the stoichiometry of 1:2 could still be observed. The structure of $(\text{HO}-\text{H}-\text{OH})^-$ was discussed by Gronert before.⁴

The quenching mechanisms are tentatively explained in Fig. 8. As we discussed before, structural relaxation of the S_1 excited state of **1** would result an internal charge transfer (ICT) excited state, which is denoted as ICT (S_1). Fluorescence from this ICT (S_1) state to the ground state (S_0) is allowed to give emission at 430 nm. However, after the $(\mathbf{1} \cdot \text{F}_2)^{2-}$ formation, excessive negative-charges are localized onto the oxygen atoms. The energy level of the oxygen lone-pair would therefore be significantly raised and becomes the HOMO. The emission behavior will therefore be governed by the BINOL subunit. Instead of the original light emissive mechanism, now the π^* (BINOL) to n (BINOL) transition becomes the predominant relaxation pathway. This is usually a radiationless transition due to the presence of the plentiful thermal relaxation pathways through hydrogen bond and electrostatic interactions, which is known as the static quenching phenomenon.¹⁰³

Although the induced fluorescence quenching ability of OAc^- , H_2PO_4^- , and OTs^- is relatively weak in comparison to F^- , the fluorescence changes are still observable under the experimental conditions. On the other hand, no significant fluorescent quenching was observed when Cl^- , Br^- , I^- , or HSO_4^- had been introduced up to 500 M equiv. Therefore, the selectivity of the F^- induced fluorescence quenching is very high. Among the anions we tested, as shown in Fig. 9, F^- is the most sensitive anion that could effectively induce the fluorescence quenching at low concentration. Other anions including OAc^- and H_2PO_4^- are competitors for **1**. However, the sensitivity is much lower.

To shed more light on the complexation site, the binding studies of **1**, **2**, and **3** were carried out for comparison. Compound **2** has only one OH group available while **3** has both of the OH groups being benzylated. Neither **2** nor **3** could have the same level of sensitivity towards the fluoride ion induced fluorescent quenching phenomenon. These observations strongly suggested that both OH groups on the BINOL subunit are crucial for creating the fluoride complexation.

On the other hand, oxoanions including OAc^- , H_2PO_4^- , and OTs^- were found to bind in a 1:1 fashion. For example, the linear-plot of I_0/I_i versus $[\text{H}_2\text{PO}_4^-]$ obeys the equation of

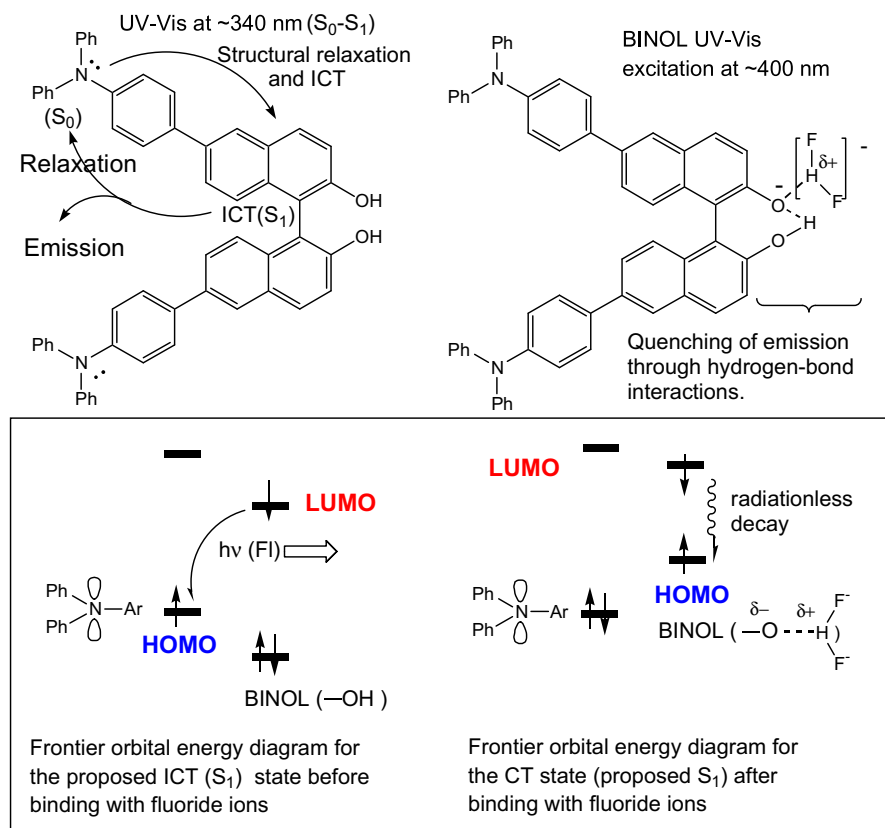


Fig. 8. Proposed fluorescence quenching through fluoride complexation.

$$[\text{H}_2\text{PO}_4^-] \cdot \beta_1^{\text{HP}} = \frac{[(1 \cdot \text{H}_2\text{PO}_4^-)]}{[1]} = \frac{I_0 - I_i}{I_i} = \frac{I_0}{I_i} - 1,$$

with the value of $\log \beta_1^{\text{HP}} = 4.87 \pm 0.03$ was obtained. By using the same strategy, the constants of $\log \beta_1^{\text{OAc}} = 5.13 \pm 0.02$ for OAc^- , and $\log \beta_1^{\text{OTs}} = 3.36 \pm 0.02$ for OTs^- (tetraethylammonium (TEA) salt) were therefore estimated.

2.4.3. *Back-titration experiments with Cl^-* . Chloride displays a more intricate behavior. Although there were no changes in the UV-vis and fluorescence spectra upon addition of Cl^- , the binding of **1** with Cl^- could be detected by competition experiments against F^- binding. In this experiment, the fluorescence of **1** originally suppressed by complexation with F^- (20 M equiv) would be gradually resumed upon addition of chloride ions. The sigmoidal pattern of

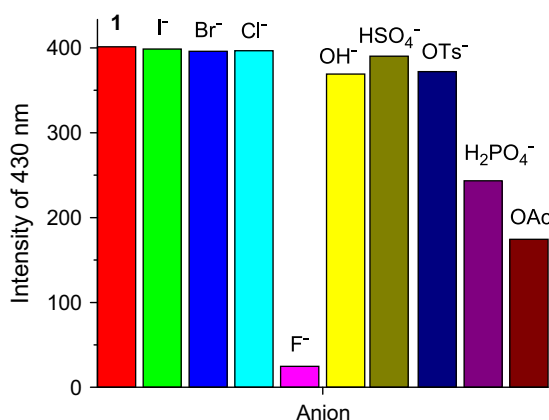
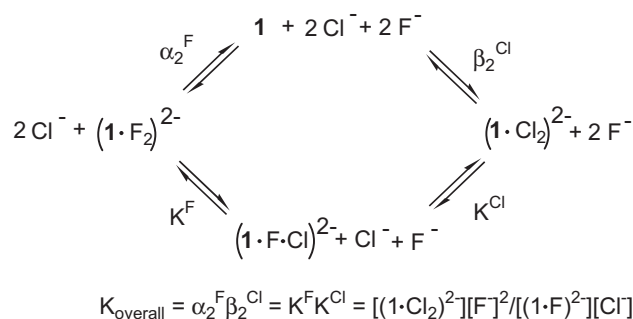


Fig. 9. Fluorescence intensity change of **1** by addition of anions (8 equiv).

the plot of the fluorescence intensity versus $[\text{Cl}^-]/[\text{F}^-]$ strongly suggested a high order complexation. The schematic diagram is tentatively proposed in Scheme 4.



Scheme 4. Competitive complexation between chloride and fluoride ions.

In the presence of excess amounts of Cl^- , halo-ion exchange would occur to give rise to $(1 \cdot \text{Cl} \cdot \text{F})^{2-}$ and $(1 \cdot \text{Cl}_2)^{2-}$. Although the equilibria about the dissociative mechanisms through **1** might still exist, the concentrations of **1** and the related intermediates $(1 \cdot \text{F})^{-1}$ and $(1 \cdot \text{Cl})^{-1}$ should be low. Therefore, $(1 \cdot \text{Cl} \cdot \text{F})^{2-}$ and $(1 \cdot \text{Cl}_2)^{2-}$ should be the major species that response to the fluorescent measurements. Due to the lower electro-negativity of Cl^- , weak CT character in the complex is expected. Therefore, the fluorescence quenching effect will become insignificant. By assuming that the luminescence efficiency of $(1 \cdot \text{Cl} \cdot \text{F})^{2-}$ and $(1 \cdot \text{Cl}_2)^{2-}$ are similar to that of **1**, the overall equilibrium constants of $K_{\text{overall}} = \alpha_2^{\text{F}} \cdot \beta_2^{\text{Cl}} = K^{\text{F}} \cdot K^{\text{Cl}} = (9.08 \pm 0.62) \times 10^{-2}$ and $K^{\text{F}} = 0.188 \pm 0.063$ could then be estimated by non-linear curve fitting of the data into the following equation.

$$\frac{I_i}{I_f - I_i} = K_{\text{overall}} \left(\frac{[\text{Cl}^-]}{[\text{F}^-]} \right)^2 + K^{\text{F}} \left(\frac{[\text{Cl}^-]}{[\text{F}^-]} \right)$$

It should be noted that α_2^{F} is a reciprocal of β_2^{F} ($\log \beta_2^{\text{F}} = 11.00 \pm 0.08$) that have been measured before, the values of $\log(\beta_2^{\text{Cl}}) = 9.96 \pm 0.11$, $\log K^{\text{F}} = -0.726 \pm 0.17$ and $\log K^{\text{Cl}} = -0.316 \pm 0.18$ could therefore be calculated.

On the other hand, the hydrogen bond accepting ability of Br^- and I^- is too low to compete against the fluoride complexation. Therefore, no changes would be observed upon addition of excess amounts of Br^- and I^- .

2.4.4. Interactions with HSO_4^- . Although weak hydrogen bond ability of HSO_4^- is expected, to our surprise, competitive binding against fluoride ions could still be observed. In the back-titration study, upon addition of HSO_4^- to the solution of $(\mathbf{1} \cdot \text{F}_2)^{2-}$, the fluorescence at 430 nm was gradually increased (Fig. 10). Nevertheless, the fluorescence intensity could not be completely recovered; only about 60% of the original intensity could be obtained in the presence of 2000 M equiv of TBAHSO₄. On the contrary, no fluorescence quenching was observed when 2000 M equiv of TBAHSO₄ was added to $\mathbf{1}$ (1×10^{-6} M) in the absence of fluoride ions. All these indicate that the formation of $(\mathbf{1} \cdot \text{HSO}_4)^-$ does not respond to the partial quenching effect. These inconsistent observations could only be explained by assuming the formation of a new complex other than $(\mathbf{1} \cdot \text{HSO}_4)^-$ in the back-titration experiments. Quantitative spectral analysis reveals that the stoichiometry of the reaction follows a 1:1 pattern, indicating that only 1 M equiv of HSO_4^- would be taken up to substitute the F^- . This could be explained by assuming the formation of a co-complex of $(\mathbf{1} \cdot \text{F} \cdot \text{HSO}_4)^{2-}$ during titration. As shown in Scheme 5, replacement of one of the fluoride ion from the $(\mathbf{1} \cdot \text{F}_2)^{2-}$ proceeds to give $(\mathbf{1} \cdot \text{F} \cdot \text{HSO}_4)^{2-}$. This equilibrium would obey the equation of

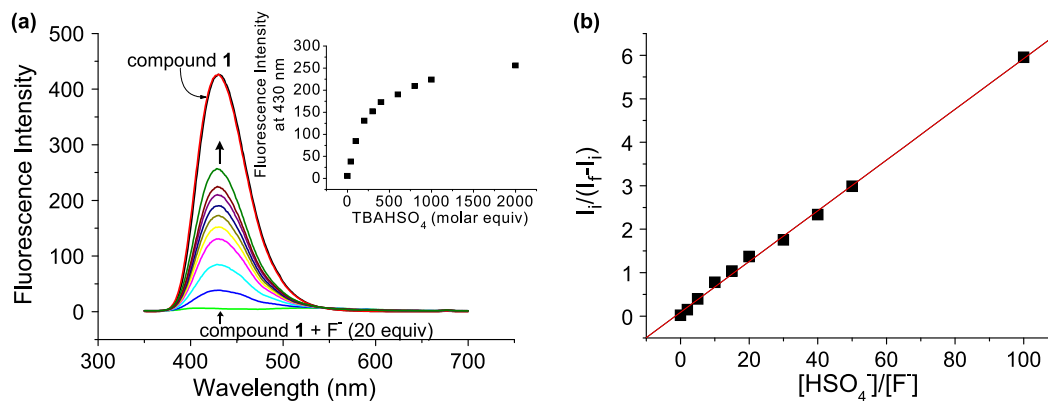


Fig. 10. (a) The traces of the fluorescence intensity in the back-titration experiments of $(\mathbf{1} \cdot \text{F}_2)^{2-}$ with HSO_4^- . The molar equivalents of $\mathbf{1}$:TBAF in the mother solution was 1:20. The molar equivalents of TBAHSO₄ added were: 0, 40, 100, 200, 300, 400, 600, 800, 1000, and 2000. (b) A linear-correlation plot of $I_i/(I_f - I_i)$ versus $([\text{HSO}_4^-]/[\text{F}^-])$ with $r^2 = 0.99$ is observed. I_f of 298 ± 1 , which is about 70% of the intensities of $\mathbf{1}$ and $(\mathbf{1} \cdot \text{HSO}_4)^-$, was determined.



No quenching in the presence of TBAHSO₄
(2000 molar equiv)



Recovery of 60% of fluorescent intensity in the
presence of TBAHSO₄ (2000 molar equiv)

Scheme 5. Competitive complexation between HSO_4^- and fluoride ions.

$\beta^{\text{FHS}} = [(\mathbf{1} \cdot \text{F} \cdot \text{HSO}_4)^{2-}][\text{F}^-] / [(1 \cdot \text{F}_2)^{2-}][\text{HSO}_4^-]$. This is reasonable due to the acidity of HSO_4^- ($\text{p}K_{\text{a}} = 1.99$)¹⁰⁴ that makes HSO_4^- also a good hydrogen bond donor as well as an acceptor. This might provide the driving force from generation of a thermodynamically stable $(\mathbf{1} \cdot \text{F} \cdot \text{HSO}_4)^{2-}$ co-complex. However, HSO_4^- is not strong enough to replace the second F^- from the complex. The equation could be rearranged so that $[\text{HSO}_4^-]/[\text{F}^-] \cdot \beta^{\text{FHS}} = (\mathbf{1} \cdot \text{F} \cdot \text{HSO}_4)^{2-} / [(1 \cdot \text{F}_2)^{2-}] = I_i/(I_f - I_i)$, whereas I_i is the fluorescence intensity in the presence of i molar equivalents of TBAHSO₄, and I_f is the final limit of the fluorescent intensity, and β^{FHS} is the equilibrium constant for the reaction. A value of $\log(\beta^{\text{FHS}}) = -1.237 \pm 0.014$ was obtained from the linear fit in Fig. 10(b).

2.5. NMR titration

As a validation of the above prediction, the binding behavior of $\mathbf{1}$ with various anions was examined by ¹H NMR titration. Fig. 11 shows the ¹H NMR changes of $\mathbf{1}$ during titrations with F^- . The proton signals were assigned on the basis of its ¹H–¹H COSY, HMBC, HMQC, and 2D-NOESY spectra.

In the titration with F^- , the chemical shift (δ) of H(3), labeled by a red star, was first gradually downfield shifted to reach the maximum at 7.53 ppm ($\Delta\delta = 0.15$ ppm) at the 1-M equiv point, followed by turning backward to the upfield direction. These observations indicated that there are at least two stages of binding for $\mathbf{1}$ in the titration. On the contrary, only small $\Delta\delta$ shifts of -0.01 and -0.05 for H(12) and H(18) were observed, suggesting that the hydrogen bond complex formation should occur on the BINOL unit rather than on the triphenylamine units.

In comparison to the unusual shift of H(3), other protons on the naphthalene units, including $\delta_{\text{H}}(7)$, $\delta_{\text{H}}(5)$, and $\delta_{\text{H}}(4)$ shifted all the way to the upfield region. This can be accounted for by hypothesizing the complexation processes as shown in Scheme 2. The first added F^- establishes hydrogen bond interaction with the BINOL to form $(\mathbf{1} \cdot \text{F})^{1-}$.

In this stage, bond inductive effects arising from the electronegative fluoride ion makes H(3) slightly deshielded to the downfield region. On addition of the second fluoride ion, a new complex $(\mathbf{1} \cdot \text{F}_2)^{2-}$ is formed, in which the proton transfer proceeds more advanced in that stage, leading to more negative-charges residing onto the BINOL. This is probably due to the particular stability of the $(\text{HF}_2)^{1-}$ dimer, for which the highest hydrogen bond energy has been calculated (39 kcal/mol) in the gas phase.¹⁰⁵ The second F^- acts as a very strong base, capable of abstracting the proton from the BINOL subunit. This assumption was consistent with our crystallographic study in which the BINOL anion could be observed in the co-crystal structure. Under these circumstances, all the protons on the BINOL subunit, including

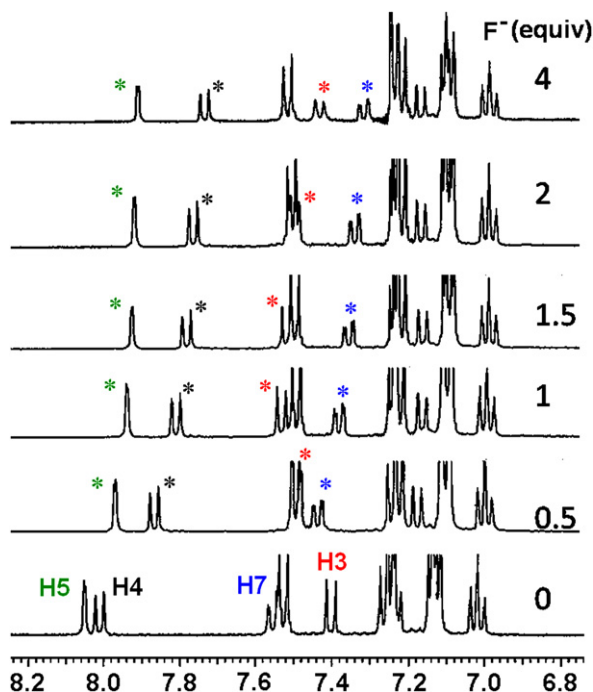


Fig. 11. Spectral changes of the ^1H NMR in the titration experiments of **1** with TBAF.

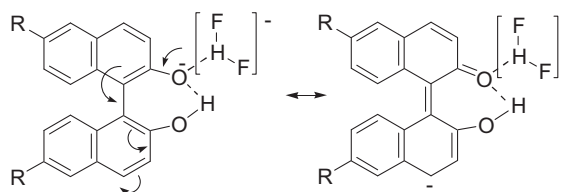
$\delta_{\text{H}}(3)$, becomes more shielded. However, due to the relatively low polarity of CDCl_3 , the $(\text{HF}_2)^{-}$ moiety might still be attached to the BINOL anion through hydrogen bond interactions.

Although only the 1:1 complex with OAc^- had been observed by fluorescence spectrometry, higher order stoichiometry was observed in the ^1H NMR. The δ of H(3) was first downfield shifted to the maximum at δ 7.47 ($\Delta\delta=0.09$) at around 1-M equiv point, followed by turning backward to the upfield direction. Recently, it has been proposed about the formation of $[\text{CH}_3\text{CO}_2\text{H}\cdots\text{O}_2\text{CCH}_3]^-$ in the study of squaramide anion recognition,¹⁰⁶ and evidenced in solid state by neutron-diffraction experiment.¹⁰⁷

The addition of H_2PO_4^- into a CDCl_3 solution of **1** also resulted in significant perturbations of the most notably protons of H(4) and H(3) that are adjacent to the OH group. While H(4) is progressively upfield shifted by 0.26 ppm, H(3) is progressively downfield shifted by about 0.2 ppm. This result again demonstrated the hydrogen bond complexation of **1** with H_2PO_4^- . With regard to the multiple hydrogen binding ability of oxoanions, it is easy to perceive that H_2PO_4^- would bind with **1** in a 1:1 manner as shown in Scheme 4. Although proton transfer from the BINOL subunit to H_2PO_4^- is expected due to the observation of the CT band at 400 nm in UV–vis titration experiments, the electron-density delivered from the H_2PO_4^- mono-anion is lower due to its weaker basicity in comparison to that from the two F^- ions. Therefore, the π -electron density localized at C(3) are expected to be low so that $\Delta\delta$ of H(3) is mainly governed by the inductive effects. Under this circumstance, H(3) shifts all the way to the downfield region and the reverse trend back to the deshielding region has not been observed in this case. Similarly, binding of **1** with Cl^- , Br^- , I^- , and HSO_4^- in CDCl_3 was again evidenced by ^1H NMR experiments. Upon addition of the anions to **1**, similar trends of δ shifts as described in the H_2PO_4^- studies were observed.

It is noteworthy to mention that the titration limits of $\Delta\delta$ for the H(4) in the NMR titrations with TBAF, TBAOAc, TBAH_2PO_4 , TBACl, TBAHSO_4 , TBABr, and TBAI are valuable parameters to study. In our experiments, the values of -0.305 , -0.286 , -0.250 , -0.182 , -0.132 , -0.134 , and -0.071 were recorded, respectively. The shielding effect on H(4) may arise from the increasing electron-density on the oxygen atoms delocalization to C(4) according to the Solntsev and

Tolbert model (Scheme 6).¹⁰⁶ This model is consistent with our X-ray crystallographic data of the anionic BINOL A, in which the short bond length of O(5)–C(41) was observed, implying the partial π bond character as suggested in the resonance structures. In addition, the field effect arising from the negatively charged oxygen atoms may also have major contribution to the shielding of H(4). Therefore, the empirical trends of the $\Delta\delta$ may become a useful tool to elucidate the electron-density on the oxygen atoms.



Scheme 6. Proposed electronic-delocalization of the charge-density on the oxygen atom to C(4) according to the Solntsev and Tolbert model.¹⁰⁶

Among the anions we studied, $(\text{F}_2)^{2-}$ has the highest $\Delta\delta$ of -0.3 , indicating that the electron-density on the oxygen atoms is the highest one. On the other hand, H_2PO_4^- has $\Delta\delta$ of -0.26 , suggesting that there is slightly lesser electron-density on the oxygen atoms. This observation again suggested that proton transfer on $(\text{H}_2\text{PO}_4)^{1-}$ may take place so that the resonance form of $-\text{O}^- \cdots \text{HO}(\text{P}=\text{O})(\text{OH})_2$ is highly significant. On the contrary, $(\text{Cl})^{2-}$ and $(\text{HSO}_4)^{1-}$ have lesser the $\Delta\delta$ of -0.182 and -0.132 , suggesting that there is lesser electron-density on the oxygen atoms. This could also explain why no CT band could be observed in the UV–vis titration experiments with Cl^- and HSO_4^- . Similarly, addition of TBABr and TBAI to **1** does lead to the observation of $\Delta\delta$ shifts of -0.134 and -0.071 , even the values are relatively small. Therefore, complexation could still be concluded.

2.6. Aspects about the hydrogen bond complexation

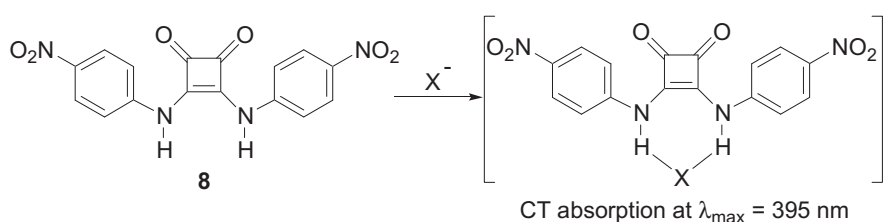
The sensory behavior of **1** with anions is intriguing. The order of the apparent quenching ability of $\text{F}^- > \text{OAc}^- > \text{H}_2\text{PO}_4^- > \text{OH}^- > \text{OTs}^- > \text{HSO}_4^-$, Cl^- , Br^- , I^- is more or less parallel to the order of the intrinsic basicity, indicating that the basicity, besides the hydrogen bond ability, should play some roles on the equilibria. One final question has to be addressed is that whether dissociation of the proton-transfer complex would occur to give the BINOL free anion. Indeed, dissociation of the proton-transfer complexes has been reported in literature. For example, careful studies about the equilibria between hydrogen bonding association and deprotonation processes in urea, thiourea, and amide derivatives in polar solvents, such as DMSO and acetonitrile revealed that the presence of the dissociative equilibrium would affect the measurement of the binding constants.^{47,52,55} Usually, deprotonation and dissociation of the complexes would be more significant at dilute conditions and therefore the dissociation process should be concentration dependent. However, the formation constant we obtained for $[\text{H}_2\text{PO}_4]$ at different concentrations are in comparable order of magnitude; the value of $\log \beta_{11}^{\text{HP}}$ of 4.36 ± 0.01 was obtained from UV titration at 1×10^{-5} M while similar value of $\log \beta_{11}^{\text{HP}}$ of 4.87 ± 0.03 was recorded from fluorescence titration at 1×10^{-6} M. This observation suggested that the dissociation effects are relatively mild. This might be due to the lower polarity of the solvents of CH_2Cl_2 and CDCl_3 used in the studies, in which hydrogen bond association interactions become more significant. It is noteworthy to point out that the final ^1H NMR spectra of the complexes in titration with different anions are all different. If the BINOL free anion is formed as the final product, one might expect to see similar final spectra in all titrations.

It is noteworthy to remind that the mono-benzylated **2** does not show comparable responses when comparing to **1**. If the fluorescence

quenching is mainly arising from the acid–base equilibria, one might expect that **2**, containing one naphtholic proton, should show similar response, which is contradicting to the present observations. All these strongly suggested that the observed phenomena could not be explained by the simple acid–base mechanisms.

Although addition of Cl^- does not lead to any significant change on the absorption or fluorescence spectra, binding behavior was clearly evidenced on the basis of the ^1H NMR analysis as well as in the competitive experiments. If the previously described red-shifted absorption and fluorescence quenching phenomena are really originated from the formation of free anion of $\mathbf{1}^-$, halo-exchange of the F^- with Cl^- on HF_2^- should not be able to resume the fluorescence of **1**. This observation implies that the F^- ions are bound to **1**. It is noteworthy to re-emphasize that CH_2Cl_2 and CDCl_3 are relatively non-polar solvents. Therefore, it is not surprise to see that even weak interactions, such as hydrogen bond interactions could become predominant in complex formation.

Recently, Fabbri reported the study of squaramide **8** for anion recognition.¹⁰⁸ Squaramide **8** has a hydrogen bond induced charge-transfer absorption centered at 395 nm. Upon additions of anions, red-shift ($\Delta\lambda$ in nm) of the charge-transfer bands was observed. The values of $\Delta\lambda=27, 16, 13,$ and 6 nm were reported for the F^- , Cl^- , Br^- , and I^- complexation, respectively (Scheme 7). These values were found to be linearly correlated to the $\log K$ of the squaramide hydrogen bond complexation. Therefore, the $\Delta\lambda$, which refers to the hydrogen bond strength, are reliable parameters that could be used to reflect the extents of the hydrogen bond interactions. Fig. 12 discloses the existence of a linear correlation between the upfield-shift value of $\Delta\delta$ for the H(4) of **1** versus $\Delta\lambda$ values of **8**. The correlation strongly suggested that



Scheme 7. Binding of halides with squaramide **8**.

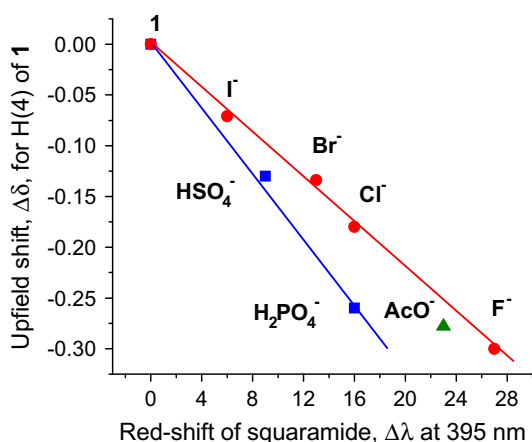


Fig. 12. Plot of $\Delta\delta$ for the H(4) of **1** versus $\Delta\lambda$ of **8** at 395 nm.

the binding mode of **1** for all halide ions belongs to the same type of complexation mechanisms, which are governed by hydrogen bond interactions. On the other hand, H_2PO_4^- and HSO_4^- fall onto another correlation line. This is consistent with our previous conclusions that the binding modes for oxoanions are different from that of simple

halide ions. It is noteworthy to point out the observation of the unusual turning of $\Delta\delta$ of H(3) for OAc^- , which indicates the formation of the $(\mathbf{1} \cdot (\text{OAc})_2)^{2-}$ in the NMR titration. Therefore, it is no surprise that the value of $\Delta\delta(\text{OAc})$ for the H(4) falls onto the line of halogens, which is the characteristic properties of the family of $(\mathbf{1} \cdot \text{X}_2)^{2-}$.

3. Conclusions

In summary, we demonstrated that BINOL can be a useful building block in the design and synthesis of neutral receptors for anions. Although BINOL is known to be an interest molecule in organic synthesis, its binding behavior with anions has not been systematically evaluated before. By taking the advantage of the fluorescence properties of **1**, interesting binding behavior of BINOL has now be elucidated in the present work. For a long time, chemists are interested in studying proton transfer in a hydrogen bond complex. However, the study would sometime be interfered by complex dissociation. In our study, we adopted the use of the hydrogen bond induced $\Delta\lambda$ on the CT band of squaramide as a probe in the correlation analysis, and evidenced that proton transfer through hydrogen bond interactions is crucial in our cases, even BINOL is considered as a relatively acidic species.

4. Experimental

4.1. General about the synthetic procedures

The compounds are prepared according to the literature methods as cited in the references. All reagents commercially available were purchased and used directly.

4.1.1. 2'-(Benzyloxy)-6,6'-dibromo-1,1'-binaphthyl-2-ol (**6**). To a mixture of **4** (2.04 g, 4.62 mmol), K_2CO_3 (2.81 g, 20.3 mmol), and 18-crown-6 (0.10 g, 0.38 mmol) in acetone (40 mL) was added dropwise benzyl bromide (0.6 mL, 5.05 mmol). The mixture was refluxed for 48 h. After removal of the acetone, a mixture of H_2O (50 mL) and CH_2Cl_2 (50 mL) was added. The aqueous layer was extracted with CH_2Cl_2 (3×50 mL). All of the organic extracts were combined and dried over anhydrous MgSO_4 . The extracts were concentrated to give crude **6** that was further purified by liquid column chromatography on silica gel, using CH_2Cl_2 /hexane (50% v/v) as the eluent to give of **6** (1.24 g, 50%). ^1H NMR (400 MHz, CDCl_3) δ 8.01 (t, $J=2$ Hz, 2H), 7.87 (d, $J=9$ Hz, 1H), 7.81 (d, $J=9$ Hz, 1H), 7.46 (d, $J=9$ Hz, 1H), 7.35 (d, $J=9$ Hz, 1H), 7.32 (dd, $J=9, 2$ Hz, 1H), 7.26 (dd, $J=9, 2$ Hz, 1H), 7.19–7.17 (m, 3H), 7.03–7.00 (m, 3H), 6.86 (d, $J=9$ Hz, 1H), 5.08 (d, $J=6$ Hz, 2H), 4.89 (s, 1H); ^{13}C NMR (100 MHz, CDCl_3) δ 155.1, 151.7, 136.5, 132.5, 132.2, 130.7, 130.6, 130.3, 130.1, 130.0, 129.8, 129.1, 128.4, 127.9, 126.8, 126.6, 126.5, 118.7, 118.4, 117.1, 116.7, 116.4, 114.8, 71.1; HRMS (FAB): m/z calcd for $\text{C}_{27}\text{H}_{18}^{79}\text{Br}_2\text{O}_2$ 531.9674, found 531.9670.

4.1.2. 2,2'-Bis(benzyloxy)-6,6'-dibromo-1,1'-binaphthyl (**7**). To a mixture of **4** (18.0 g, 40.7 mmol), K_2CO_3 (35.0 g, 252 mmol), and 18-crown-6 (0.80 g, 3.03 mmol) in acetone (400 mL), benzyl bromide (12.0 mL, 101 mmol) was added dropwise. The mixture was refluxed for 48 h. After removing acetone, a mixture of H_2O (300 mL) and

CH₂Cl₂ (300 mL) was added. The aqueous layer was extracted with additional portions of CH₂Cl₂ (3×300 mL). All of the organic extracts were combined and dried over anhydrous MgSO₄. After removal of the organic solvents, the solid obtained was washed with methanol to give **7** (14.2 g, 56%). ¹H NMR (400 MHz, CDCl₃) δ 8.04 (d, *J*=2 Hz, 2H), 7.83 (d, *J*=9 Hz, 2H), 7.44 (d, *J*=9 Hz, 2H), 7.31 (dd, *J*=9, 2 Hz, 2H), 7.12–7.20 (m, 6H), 7.05 (d, *J*=9 Hz, 2H), 6.99 (d, *J*=7 Hz, 2H), 5.06 (s, 4H); ¹³C NMR (100 MHz, CDCl₃) δ 154.3, 137.0, 132.5, 130.4, 129.8, 129.7, 128.6, 128.2, 127.4, 127.1, 126.6, 120.2, 117.5, 116.6, 70.9; HRMS (FAB): *m/z* calcd for C₃₄H₂₄⁷⁹Br₂O₂ 622.0143, found C₃₄H₂₄⁸¹Br₂O₂ 626.0110.

4.1.3. 6,6'-Bis(4-(diphenylamino)phenyl)-1,1'-binaphthyl-2,2'-diol (1). To a mixture of **4** (4.84 g, 11.0 mmol), 4-(diphenylamino)phenylboronic acid (**5**) (10.0 g, 34.6 mmol), K₂CO₃ (10.0 g, 72.4 mmol), and Pd(PPh₃)₄ (2.00 g, 1.37 mmol) were added H₂O (10 mL) and toluene (100 mL). The mixture was refluxed for 24 h. After the reaction was completed, additional amounts of water (200 mL) were added. The aqueous layer was extracted with CH₂Cl₂ (4×200 mL). The organic extracts were combined and dried over (anhydrous MgSO₄) and concentrated. The product was purified by liquid column chromatography on silica gel, using CH₂Cl₂/hexane (1:1) as the eluent to give a solid, which was washed with pentane to give pure **1** (12.7 g, 32%). ¹H NMR (400 MHz, CDCl₃) δ 8.06 (2H), 7.98 (d, *J*=9 Hz, 2H), 7.54–7.58 (m, 6H), 7.38 (d, *J*=9 Hz, 2H), 7.26–7.30 (m, 10H), 7.15–7.21 (m, 12H), 7.05 (t, *J*=7 Hz, 4H), 5.15 (br s, 2H); ¹³C NMR (100 MHz, CDCl₃) δ 152.4, 147.4, 147.0, 136.2, 134.4, 132.1, 131.4, 129.6, 129.1, 127.7, 126.7, 125.4, 124.6, 124.3, 123.8, 122.8, 118.1, 110.8; HRMS (FAB): *m/z* calcd for C₅₆H₄₀N₂O₂ 772.3090, found 772.3083. Anal. Calcd C₅₆H₄₀N₂O₂: C, 87.02; H, 5.22; N, 3.62, found C, 86.66; H, 5.06; N, 3.49.

4.1.4. 2'-(Benzyloxy)-6,6'-bis(4-(diphenylamino)phenyl)-1,1'-binaphthyl-2-ol (2). To a mixture of **6** (1.24 g, 2.32 mmol), **5** (2.00 g, 6.92 mmol), K₂CO₃ (2.30 g, 16.64 mmol), and Pd(PPh₃)₄ (0.20 g, 0.17 mmol) were added H₂O (1 mL) and toluene (10 mL). The mixture was refluxed for 24 h. Additional amounts of water (20 mL) and CH₂Cl₂ (30 mL) were then added. The aqueous layer was extracted with CH₂Cl₂ (4×30 mL). The organic extracts were combined, dried (anhydrous MgSO₄), and concentrated (rotary evaporation). The crude product was purified by liquid column chromatography on silica gel, using CH₂Cl₂/toluene (17% v/v) as the eluent to give **2** (0.74 g, 37%). ¹H NMR (400 MHz, CDCl₃) δ 8.04 (d, *J*=4 Hz, 2H), 8.00 (d, *J*=9 Hz, 1H), 7.96 (d, *J*=9 Hz, 1H), 7.54 (t, *J*=9 Hz, 5H), 7.46–7.49 (m, 2H), 7.39 (d, *J*=9 Hz, 1H), 7.31 (d, *J*=10 Hz, 1H), 7.24–7.28 (m, 8H), 7.13–7.18 (m, 16H), 7.06–7.08 (m, 2H), 7.02 (t, *J*=7 Hz, 4H), 5.11 (d, *J*=5 Hz, 2H), 5.01 (s, 1H); ¹³C NMR (100 MHz, CDCl₃) δ 154.9, 151.3, 147.7, 147.6, 147.3, 146.9, 136.9, 136.7, 135.5, 134.6, 133.0, 131.0, 130.1, 129.5, 129.3, 129.2, 128.3, 127.8, 127.7, 126.9, 126.7, 125.8, 125.6, 125.5, 125.4, 125.2, 124.5, 124.4, 124.0, 123.9, 123.0, 122.9, 118.0, 116.4, 115.1, 71.3; HRMS (FAB): *m/z* calcd for C₆₃H₄₆N₂O₂ 862.3559, found 862.3549. Anal. Calcd C₆₃H₄₆N₂O₂: C, 87.67; H, 5.37; N, 3.25, found C, 87.28; H, 5.14; N, 3.06.

4.1.5. 2,2'-Bis(benzyloxy)-6,6'-bis(4-(diphenylamino)phenyl)-1,1'-binaphthyl (3). To a mixture of **7** (4.02 g, 6.46 mmol), **5** (9.37 g, 32.4 mmol), K₂CO₃ (10.0 g, 72.4 mmol), and Pd(PPh₃)₄ (1.49 g, 1.29 mmol) were added H₂O (10 mL), ethanol (5 mL), and toluene (30 mL). The mixture was refluxed for 24 h. Additional portions of H₂O (100 mL) and CH₂Cl₂ (200 mL) were added. The aqueous layer was extracted with CH₂Cl₂ (3×200 mL). The extracts were washed, dried (anhydrous MgSO₄), concentrated, and purified by column chromatography on silica gel, eluting with 10% (v/v) of CH₂Cl₂/hexane to give **3** (2.83 g, 46%). ¹H NMR (400 MHz, CDCl₃) δ 8.04 (d, *J*=2 Hz, 2H), 7.96 (d, *J*=9 Hz, 2H), 7.56 (d, *J*=9 Hz, 4H), 7.49 (dd, *J*=9, 2 Hz, 2H),

7.43 (d, *J*=9 Hz, 2H), 7.23–7.31 (m, 10H), 7.07–7.16 (m, 16H), 6.99–7.04 (m, 8H); ¹³C NMR (100 MHz, CDCl₃) δ 153.9, 147.5, 146.8, 137.3, 135.7, 135.0, 133.0, 129.6, 129.4, 129.1, 128.0, 127.7, 127.2, 126.6, 126.0, 125.7, 125.0, 124.2, 123.9, 122.7, 120.5, 116.3, 71.2; HRMS (FAB): *m/z* calcd for C₇₀H₅₂N₂O₂ 952.4029, found 952.4041. Anal. Calcd C₇₀H₅₂N₂O₂: C, 88.21; H, 5.50; N, 2.94, found C, 88.16; H, 5.63; N, 2.56.

4.2. Binding constant measurements

4.2.1. UV-vis and fluorescence experimental procedures. All chemicals were heated to dry in vacuum before use. The solvents were dried according to the standard procedure and distilled before use. The samples were weighed, transferred, and prepared in a dry-box in order to avoid any interference from moisture. The measurements were handled at 296 K without other notice. In the UV-vis absorption experiments, the binding of **1** with F⁻ is too strong to estimate accurately. However, the 1:1 binding constant of **1** with H₂PO₄⁻, could be estimated according to the expression as follows.

$$[\text{H}_2\text{PO}_4^-] \cdot \beta_1^{\text{HP}} = \frac{[(\mathbf{1} \cdot \text{H}_2\text{PO}_4^-)]}{[\mathbf{1}]} = \frac{A_i}{A_f - A_i}$$

The value of the binding constant β_1 could therefore be estimated from the plot.

4.2.2. Fluorescence analysis about the fluoride binding. The proposed equilibria are shown in Scheme 3, in which $\beta_2^{\text{F}} = K_1^{\text{F}} \cdot K_2^{\text{F}} = [(\mathbf{1} \cdot \text{F}_2)^{2-}] / ([\mathbf{1}] [\text{F}^-]^2)$. To avoid the interference arising from CT band absorption tailing to 450 nm, the fluorescence data at 470 nm were adopted for the quantitative analysis. However, the deviation was found to be small. The deviation of β_2^{F} value was within 10% when comparison to that from 430 nm. The inset in Fig. 7 shows the fluorescence quenching during titration a 470 nm. When the dosage of F⁻ was less than 1 M equiv, the fluorescent intensity almost unchanged, indicating that formation of (1·F)⁻ does not lead to any significant fluorescence quenching effect. On the other hand, upon addition of excess F⁻, the intensity gradually fades away. This observation is consistent with efficiency, and (1·F₂)²⁻ would lead to complete luminescence quenching due to its charge-transfer character, the mathematical expression could be derived as follow:

(1) The intensity equations could be expressed as follows, by assuming that the emission intensity proportional constants of Φ_1 and $\Phi_{1 \cdot \text{F}}$ are almost identical.

$$I_i = [\mathbf{1}] \Phi_1 + [(\mathbf{1} \cdot \text{F})^-] \Phi_{1 \cdot \text{F}} \approx ([\mathbf{1}] + [(\mathbf{1} \cdot \text{F})^-]) \Phi_1$$

(2) The intensity ratio equation could be written as follows.

$$\begin{aligned} \frac{I_0 - I_i}{I_i} &= \frac{[\mathbf{1}]_0 \Phi_1 - ([\mathbf{1}] + [(\mathbf{1} \cdot \text{F})^-]) \Phi_1}{([\mathbf{1}] + [(\mathbf{1} \cdot \text{F})^-]) \Phi_1} \\ &= \frac{[(\mathbf{1} \cdot \text{F}_2)^{2-}]}{[\mathbf{1}] + [(\mathbf{1} \cdot \text{F})^-]} \\ &= \frac{\beta_2^{\text{F}} [\mathbf{1}] [\text{F}^-]^2}{[\mathbf{1}] + K_1^{\text{F}} [\mathbf{1}] [\text{F}^-]} \\ &= \frac{\beta_2^{\text{F}} [\text{F}^-]^2}{1 + K_1^{\text{F}} [\text{F}^-]} \end{aligned}$$

Non-linear curve fitting of the data to the equation gave $\log \beta_2^{\text{F}} = 11.00 \pm 0.08$ while $\log K_1^{\text{F}} = 4.43 \pm 0.11$. The data fit well with

this equation up 75% of intensity quenching. Similar data treatments were carried for OH⁻ and log $\beta_2^{\text{OH}^-} = 9.05 \pm 0.01$ and log $K_1^{\text{OH}^-} = 3.86 \pm 0.42$ were obtained.

For OAc⁻, H₂PO₄⁻, and TSO⁻ titrations, the data obey the model with the stoichiometry of 1:1, which is different from that of the fluoride and hydroxide ions. The equation could be expressed as follows.

$$[\text{H}_2\text{PO}_4^-] \cdot \beta_1^{\text{HP}} = \frac{[(\mathbf{1} \cdot \text{H}_2\text{PO}_4^-)]}{[\mathbf{1}]} = \frac{I_o - I_i}{I_i} = \frac{I_o}{I_i} - 1$$

The value of the binding constant β_1 could therefore be estimated from the plot.

4.2.3. Back-titration experiments with Cl⁻. Analysis of the data revealed that a model about formation of (1·Cl₂)²⁻ complex, as shown in Scheme 6, does provide the best fit with the data. As shown in Scheme 6, the equilibrium should lead to an expression denoted as follows.

$$K_{\text{overall}} = K^{\text{F}} \cdot K^{\text{Cl}} = \alpha_2^{\text{F}} \cdot \beta_2^{\text{Cl}} = \frac{[(\mathbf{1} \cdot \text{Cl}_2)^{2-}][\text{F}^-]^2}{[(\mathbf{1} \cdot \text{F}_2)^{2-}][\text{Cl}^-]^2}$$

The equation could then be re-written as

$$\frac{[(\mathbf{1} \cdot \text{Cl}_2)^{2-}]}{[(\mathbf{1} \cdot \text{F}_2)^{2-}]} = (\alpha_2^{\text{F}} \beta_2^{\text{Cl}}) \frac{[\text{Cl}^-]^2}{[\text{F}^-]^2}$$

On the other hand, according to the associative equilibrium,

$$K^{\text{F}} = \frac{[(\mathbf{1} \cdot \text{Cl} \cdot \text{F})^{2-}][\text{F}^-]}{[(\mathbf{1} \cdot \text{F}_2)^{2-}][\text{Cl}^-]}$$

so that the mathematical expression of

$$\frac{[(\mathbf{1} \cdot \text{Cl} \cdot \text{F})^{2-}]}{[(\mathbf{1} \cdot \text{F}_2)^{2-}]} = K^{\text{F}} \frac{[\text{Cl}^-]}{[\text{F}^-]}$$

is valid. In the back-titration experiments, the fluorescence responses mainly arise from the emission of (1·Cl·F)²⁻ and (1·Cl₂)²⁻. The final emission intensity (I_f) of (1·Cl₂)²⁻ was determined in an independent experiment by addition of 500 M equiv of TBACl to **1**. The intensity of $I_f = 394.4$ was measured, which is very close to the original intensity of 401 for **1**. Since the quenching effect is mainly arising from the CT properties of the (1·F₂)²⁻ complex, halo-ion exchange from F⁻ to Cl⁻ would significantly reduce the CT character on (1·Cl·F)²⁻ and (1·Cl₂)²⁻. Therefore, it is reasonable to assume that the fluorescent efficiency of (1·Cl·F)²⁻ and (1·Cl₂)²⁻, denoted as $\Phi_{(1 \cdot \text{Cl} \cdot \text{F})}$ and $\Phi_{(1 \cdot \text{Cl} \cdot \text{Cl})}$ are close to that of **1** (Φ_1). On the basis of this assumption, the equation of

$$\begin{aligned} \frac{I_i}{I_f - I_i} &\sim \frac{\{[(\mathbf{1} \cdot \text{Cl}_2)^{2-}] + [(\mathbf{1} \cdot \text{Cl} \cdot \text{F})^{2-}]\} \Phi_1}{\left\{ \frac{[(\mathbf{1} \cdot \text{Cl}_2)^{2-}]_f}{[\text{F}^-]} - [(\mathbf{1} \cdot \text{Cl}_2)^{2-}] - [(\mathbf{1} \cdot \text{Cl} \cdot \text{F})^{2-}] \right\} \Phi_1} \\ &= \frac{[(\mathbf{1} \cdot \text{Cl}_2)^{2-}] + [(\mathbf{1} \cdot \text{Cl} \cdot \text{F})^{2-}]}{[(\mathbf{1} \cdot \text{F}_2)^{2-}]} \\ &= K_{\text{overall}} \left(\frac{[\text{Cl}^-]}{[\text{F}^-]} \right)^2 + K^{\text{F}} \left(\frac{[\text{Cl}^-]}{[\text{F}^-]} \right) \end{aligned}$$

could be derived. The non-linear curve fitting gave K_{overall} and K^{F} . Since $K_{\text{overall}} = \alpha_2^{\text{F}} \cdot \beta_2^{\text{Cl}} = K^{\text{F}} \cdot K^{\text{Cl}}$ and $\beta_2^{\text{Cl}} = 1/\alpha_2^{\text{F}}$ has been determined

in previous experiments, the equilibrium constant of β_2^{Cl} and K^{Cl} could be then calculated.

Acknowledgements

We thank the National Science Council of Taiwan (NSC 95-2113-M002-021-MY3, NSC 98-2119-M002-006-MY3 and NSC 97-3114-M002-005), Academia Sinica (Thematic Project), Ministry of Education of Taiwan, and National Taiwan University for financial support. We are indebted to Prof. Tahsin Chow, Prof. Sheng-Hsien Chiu, Prof. Hsiu-fu Hsu, and Prof. Wann-yin Lin for their invaluable suggestion and discussion. We also thank Mr. Gene-Hsiang Lee, Mr. Yi-Hung Liu, and Professor Shie-Ming Peng for their excellent X-ray-crystallographic service.

Supplementary data

Crystallographic data (excluding structure factors) for the structures in this paper have been deposited with the Cambridge Crystallographic Data Centre as supplementary publication (CCDC 803352). Copies of the data can be obtained, free of charge, on application to CCDC, 12 Union Road, Cambridge CB2 1EZ, UK (fax: +44 1223 336033 or e-mail: deposit@ccdc.cam.ac.uk). Supplementary data associated with this article, including ¹H and ¹³C NMR spectra of **1-3**, the HMBC, HSQC, COSY, NOESY of **1**, the CIF file for **1**, the data of the PM5 calculation, non-linear curve-fitting parameters, and ¹H NMR titration data (39 pages) are provided. Supplementary data associated with this article can be found in online version at doi:10.1016/j.tet.2011.03.047. These data include MOL files and InChIKeys of the most important compounds described in this article.

References and notes

- Gates, B. D.; Xu, Q. B.; Stewart, M.; Ryan, D.; Willson, C. G.; Whitesides, G. M. *Chem. Rev.* **2005**, *105*, 1171–1196.
- Loo, Y. L.; Willett, R. L.; Baldwin, K. W.; Rogers, J. A. J. *Am. Chem. Soc.* **2002**, *124*, 7654–7655.
- Moran, I. W.; Briseno, A. L.; Loser, S.; Carter, K. R. *Chem. Mater.* **2008**, *20*, 4595–4601.
- Jortner, J. R.; Ratner, M. A. *Molecular Electronics*; Blackwell Science: Oxford, 1997.
- Tour, J. M. *Acc. Chem. Res.* **2000**, *33*, 791–804.
- Tour, J. M.; James, D. K. "Molecular electronic computing architectures" in *Nano and Molecular Electronics Handbook*; CRC: Boca Raton, Fla, 2007, pp 2/1–2/28.
- Flood, A. H.; Wong, E. W.; Stoddart, Fraser, J. *Chem. Phys.* **2006**, *324*, 280–290.
- Lehn, J.-M. *Supramolecular Chemistry*; Wiley-VCH: Weinheim, 1995; (b) Gellman, S. H. *Chem. Rev.* **1997**, *97*, 1231–1232.
- Valeur, B.; Leray, I. *Coord. Chem. Rev.* **2000**, *205*, 3–40.
- Rogers, C. W.; Wolf, M. O. *Coord. Chem. Rev.* **2002**, *233–234*, 341–350.
- Ansllyn, E. V. J. *Org. Chem.* **2007**, *72*, 687–699.
- Ushakov, E. N.; Alifimov, M. V.; Gromov, S. P. *Russ. Chem. Rev.* **2008**, *77*, 39–58.
- Kimura, K.; Sakamoto, H.; Nakamura, M. *Bull. Chem. Soc. Jpn.* **2003**, *76*, 225–245.
- Oton, F.; Tarraga, A.; Espinosa, A.; Velasco, M. D.; Molina, P. *Dalton Trans.* **2006**, *30*, 3685–3692 and references cited therein.
- For reviews, see Ref. 15–20. Schmidtchen; F. P.; Berger M. *Chem. Rev.* **1997**, *97*, 1609–1646.
- Beer, P. D. *Acc. Chem. Res.* **1998**, *31*, 71–80.
- Antonisse, M. M. G.; Reinhoudt, D. N. *Chem. Commun.* **1998**, 443–448.
- Antonisse, M. M. G.; Reinhoudt, D. N. *Electroanalysis* **1999**, *11*, 1035–1048.
- Gale, P. A. *Coord. Chem. Rev.* **2000**, *199*, 181–201.
- Beer, P. D.; Gale, P. A. *Angew. Chem., Int. Ed.* **2001**, *40*, 486–516; (a) Gale, P. A. *Coord. Chem. Rev.* **2001**, *213*, 79–125.
- Kameta, N.; Hiratani, K. *Chem. Commun.* **2005**, *6*, 725–727.
- Hagihara, S.; Gremaud, L.; Bollot, G.; Mareda, J.; Matile, S. *J. Am. Chem. Soc.* **2008**, *130*, 4347–4351.
- Pirondini, L.; Dalcanale, E. *Chem. Soc. Rev.* **2007**, *36*, 695–706.
- Basabe-Desmonts, L.; Reinhoudt, D. N.; Crego-Calama, M. *Chem. Soc. Rev.* **2007**, *36*, 993–1017.
- Gunnlaugsson, T.; Glynn, M.; Tocci-Hussey, G. M.; Kruger, P. E.; Pfeffer, F. M. *Coord. Chem. Rev.* **2006**, *250*, 3094–3117.
- Cametti, M.; Rissanen, K. *Chem. Commun.* **2009**, 2809–2829.
- Cooper, C. C.; Spencer, N.; James, T. D. *Chem. Commun.* **1998**, 1365–1366.
- Yamaguchi, S.; Shirasaka, T.; Akiyama, S.; Tamao, K. *J. Am. Chem. Soc.* **2002**, *124*, 8816–8817.

29. DiCesare, N.; Lakowicz, J. R. *Anal. Biochem.* **2002**, *301*, 111–116.
30. Kubo, Y.; Yamamoto, M.; Ikeda, M.; Takeuchi, M.; Shinkai, S.; Yamaguchi, S.; Tamao, K. *Angew. Chem., Int. Ed.* **2003**, *42*, 2036–2040.
31. Kubo, Y.; Ishida, T.; Kobayashi, A.; James, T. D. *J. Mater. Chem.* **2005**, *15*, 2889–2895.
32. Liu, Z. Q.; Shi, M.; Li, F.-Y.; Fang, Q.; Chen, Z. H.; Yi, T.; Huang, C. H. *Org. Lett.* **2005**, *24*, 5481–5484.
33. Melaimi, M.; Gabbai, F. P. *J. Am. Chem. Soc.* **2005**, *127*, 9680–9681.
34. Xu, S.; Chen, K.; Tian, H. *J. Mater. Chem.* **2005**, *15*, 2676–2680.
35. Liu, X. Y.; Bai, D. R.; Wang, S. *Angew. Chem., Int. Ed.* **2006**, *45*, 5475–5478.
36. Li, Y.; Xu, S.; Li, X.; Chen, K.; Tian, H. *Chem. Lett.* **2007**, *36*, 664–665.
37. Tan, W.; Zhang, D.; Zhu, D. *Bioorg. Med. Chem. Lett.* **2007**, *17*, 2629–2633.
38. Cao, D.; Liu, Z.; Li, G. *Sens. Actuators, B* **2008**, *133*, 489–492.
39. Xu, G.; Tarr, M. A. *Chem. Commun.* **2004**, 1050.
40. Kwon, J. Y.; Jang, Y. J.; Kim, S. K.; Lee, K.-H.; Kim, J. S.; Yoon, J. J. *Org. Chem.* **2004**, *69*, 5155–5157.
41. Esteban-Gomez, D.; Fabbri, L.; Liechelli, M. *J. Org. Chem.* **2005**, *70*, 5717–5720; (d) Bolocchi, M.; Del Boca, L.; Esteban-Gomez, D.; Fabbri, L.; Liechelli, M.; Monzani, E. *J. Am. Chem. Soc.* **2004**, *126*, 16507–16514.
42. Cho, E. J.; Ryu, B. J.; Lee, Y. J.; Nam, K. C. *Org. Lett.* **2005**, *7*, 2607–2609.
43. Descalzo, A. B.; Rurack, K.; Weisshoff, H.; Martinez-Manez, R.; Macros, M. D.; Amoros, P.; Hoffmann, K.; Soto, J. J. *J. Am. Chem. Soc.* **2005**, *127*, 184–200.
44. Otón, F.; Tarraga, A.; Espinosa, A.; Velasco, M. D.; Bautista, D.; Molina, P. *J. Org. Chem.* **2005**, *70*, 6603–6608; (h) Otón, F.; Tarraga, A.; Molina, P. *Org. Lett.* **2006**, *8*, 2107–2110.
45. Boiocchi, M.; Del Boca, L.; Esteban-Gómez, D.; Fabbri, L.; Licchelli, M.; Monzani, E. *Chem.—Eur. J.* **2005**, *11*, 3097–3104.
46. Zhao, Y.-P.; Zhao, C. C.; Wu, L. Z.; Zhang, L.-P.; Tung, C.-H.; Pan, Y.-J. *J. Org. Chem.* **2006**, *71*, 2143–2146.
47. Wu, Y.; Peng, X.; Fan, J.; Gao, S.; Tian, M.; Zhao, J.; Sun, S. *J. Org. Chem.* **2007**, *72*, 62–70.
48. Kim, E.; Kim, H. J.; Bae, D. R.; Lee, S. J.; Cho, E. J.; Seo, M. R.; Kim, J. S.; Jung, J. H. *New J. Chem.* **2008**, *32*, 1003–1007.
49. Jose, D. A.; Kumar, D. K.; Ganguly, B.; Das, A. *Org. Lett.* **2004**, *6*, 3445–3448.
50. Gunnlaugsson, T.; Davis, A. P.; O'Brien, J. E.; Glynn, M. *Org. Biomol. Chem.* **2005**, *3*, 48–56.
51. Gunnlaugsson, T.; Ali, H. D. P.; Glynn, M.; Kruger, P. E.; Hussey, G. M.; Pfeiffer, F. M.; dos Santos, C. M. G.; Tierney, J. *J. Fluoresc.* **2005**, *15*, 287–299.
52. Pérez-Casas, C.; Yatsimirsky, A. K. *J. Org. Chem.* **2008**, *73*, 2275–2284.
53. Liu, H.; Tian, H. *J. Mater. Chem.* **2005**, *15*, 2681–2686.
54. Sarkar, M.; Samanta, A. *J. Phys. Chem. B* **2007**, *111*, 7027–7033.
55. Lin, C.; Simov, V.; Drucekhammer, D. G. *J. Org. Chem.* **2007**, *72*, 1742–1746.
56. Peng, X.; Wu, Y.; Fan, J.; Tian, M.; Han, K. *J. Org. Chem.* **2005**, *70*, 10524–10531.
57. Chellappan, K.; Singh, N. J.; Hwang, I. C.; Lee, J. W.; Kim, K. S. *Angew. Chem., Int. Ed.* **2005**, *44*, 2899–2903.
58. Kumar, S.; Luxami, V.; Kumar, A. *Org. Lett.* **2008**, *10*, 5549–5552.
59. Zapata, F.; Caballero, A.; Espinosa, A.; Tarraga, A.; Molina, P. *J. Org. Chem.* **2008**, *73*, 4034–4044.
60. Black, C. B.; Andrioletti, B.; Try, A. C.; Ruiperez, C.; Sessler, J. L. *J. Am. Chem. Soc.* **1999**, *121*, 10438–10439.
61. Sessler, J. L.; Camiolo, S.; Gale, P. A. *Coord. Chem. Rev.* **2003**, *240*, 17–55.
62. Ghosh, T.; Maiya, B. G.; Wong, M. H. *J. Phys. Chem. A* **2004**, *108*, 11249–11259.
63. Lin, Y.-T.; Chen, C.-T. *Org. Lett.* **2009**, *11*, 4858–4861.
64. Lee, D. H.; Lee, K. H.; Hong, J.-I. *Org. Lett.* **2001**, *3*, 5–8.
65. Zhang, X.; Guo, L.; Wu, F.-Y.; Jiang, Y.-B. *Org. Lett.* **2003**, *5*, 2667–2670.
66. Zhao, Y.; Zhang, B.; Duan, C.; Lin, Z.; Meng, Q. *New J. Chem.* **2006**, *30*, 1207–1213.
67. Kim, S. Y.; Park, J.; Koh, M.; Park, S. B.; Hong, J.-I. *Chem. Commun.* **2009**, 4735–4737.
68. Kim, S. Y.; Hong, J.-I. *Org. Lett.* **2007**, *9*, 3109–3112.
69. Kim, T.-H.; Swager, T. M. *Angew. Chem., Int. Ed.* **2003**, *42*, 4803–4806.
70. Saravanakumar, D.; Devaraj, S.; Iyyampillai, S.; Mohandoss, K.; Kandaswamy, M. *Tetrahedron Lett.* **2008**, *49*, 127–132.
71. Huang, X.; He, Y.; Chen, Z.; Hu, C. *Chin. J. Chem.* **2009**, *27*, 1526–1530.
72. Marini, V. G.; Torri, E.; Zimmermann, L. M.; Machado, V. G. *Arkivoc* **2010**, 146–162.
73. Reis, D. C.; Machado, C.; Machado, V. G. *Tetrahedron Lett.* **2006**, *47*, 9339–9342.
74. Fan, Y.; Zhu, Y.-M.; Dai, F.-R.; Zhang, L.-Y.; Chen, Z. N. *Dalton Trans.* **2007**, 3885–3892.
75. Noyori, R. *Asymmetric Catalysis in Organic Synthesis*; Wiley: New York, NY, 1994.
76. Ojima, I. *Catalytic Asymmetric Synthesis*, 2nd ed.; Wiley: New York, NY, 2000.
77. Shibasaki, M.; Yamamoto, Y. *Multimetallic Catalysts in Organic Synthesis*; Wiley-VCH: Weinheim, 2004; p 93.
78. Pu, L. *Chem. Rev.* **1998**, *98*, 2405–2494.
79. Upadhyay, S. P.; Pissurlenkar, R. R. S.; Coutinho, E. C.; Karnik, A. V. *J. Org. Chem.* **2007**, *72*, 5709–5714.
80. Kőszegi, É.; Grün, A.; Bitter, I. *Supramol. Chem.* **2008**, *20*, 565–572.
81. Liang, X.; James, T. D.; Zhao, J. *Tetrahedron* **2008**, *64*, 1309–1315.
82. Iwanek, W.; Mattay, J. *J. Photochem. Photobiol., A* **1992**, *67*, 209–226.
83. Xu, K.-X.; Chen, P.-F.; Wang, Y.-X.; Zhao, J.; Wang, C.-J. *Supramol. Chem.* **2009**, *21*, 618–623.
84. Lin, J.; Zhang, H.-C.; Pu, L. *Org. Lett.* **2002**, *4*, 3297–3300.
85. Wang, Q.; Chen, X.; Tao, L.; Wang, L.; Xiao, D.; Yu, X.-Q.; Pu, L. *J. Org. Chem.* **2007**, *72*, 97–101.
86. Liu, H.-L.; Peng, Q.; Wu, Y.-D.; Chen, D.; Hou, X.-L.; Sabat, M.; Pu, L. *Angew. Chem., Int. Ed.* **2010**, *49*, 602–606.
87. Luxami, V.; Kumar, S. *Tetrahedron Lett.* **2007**, *48*, 3083–3087.
88. Lu, Q.-S.; Dong, L.; Li, J.; Jiang, L.; Huang, Y.; Qin, S.; Hu, C.-W.; Yu, X.-Q. *Org. Lett.* **2009**, *11*, 669–672.
89. Ito, K.; Takahashi, M.; Hoshino, T.; Nishiki, M.; Ohba, Y. *Letts. Org. Chem.* **2006**, *3*, 735–740.
90. Shimasaki, T.; Kato, S.-i.; Keiko, I.; Goto, K.; Shinmyozu, T. *J. Org. Chem.* **2007**, *72*, 1073–1087.
91. Marfo-Owusu, E.; Okuyama, K.; Noguchi, K. *Mol. Cryst. Liq. Cryst.* **2003**, *399*, 29–42.
92. Vondenhof, M.; Mattay, J. *Tetrahedron Lett.* **1990**, *31*, 985–988.
93. Li, Z. H.; Wong, M. S. *Org. Lett.* **2006**, *8*, 1499–1502.
94. Tobisu, M.; Chatani, N. D. *Angew. Chem., Int. Ed.* **2009**, *48*, 3565–3568.
95. For PM5 method, see Stewart, J. J. P. *J. Comput. Chem.* **1991**, *12*, 320–341.
96. de Silva, A. P.; Gunaratne, H. Q. N.; Gunnlaugsson, T.; Huxley, A. J. M.; McCoy, C. P.; Rademacher, J. T.; Rice, T. E. *Chem. Rev.* **1997**, *97*, 1515–1566.
97. Berlman, I. B. *J. Phys. Chem.* **1970**, *74*, 3085–3093.
98. Swiatkowski, G.; Menzel, R.; Rapp, W. *J. Lumin.* **1987**, *37*, 183–189.
99. Klock, A. M.; Rettig, W.; Hofkens, J.; van Damme, M.; De Schryver, F. C. *J. Photochem. Photobiol., A* **1995**, *85*, 11–21.
100. Rettig, W. *Angew. Chem., Int. Ed. Engl.* **1986**, *25*, 971–988.
101. Weigel, W.; Rettig, W.; Dekhtyar, M.; Modrakowski, C.; Beinhoff, M.; Schlüter, A. D. *J. Phys. Chem. A* **2003**, *107*, 5941–5947.
102. For reference of the fluorescence equation, see footnote 29.
103. For theory of fluorescence quenching, see Lakowicz, J. R. *Principles of Fluorescence Spectroscopy*, 2nd ed.; Kluwer-Plenum: New York, NY, 1999, pp 237–265.
104. Dean, J. A. *Lange's Handbook of Chemistry*, 13th ed.; McGraw-Hill: Singapore, 1987.
105. Gronert, S. *J. Am. Chem. Soc.* **1993**, *115*, 10258–10266.
106. Solntsev, K. M.; Bartolo, E.-A.; Pan, G.; Muller, G.; Bommireddy, S.; Huppert, D.; Tolbert, L. M. *Isr. J. Chem.* **2009**, *49*, 227–233.
107. Barrow, M. J.; Currie, M.; Muir, K. W.; Speakman, J. C.; White, D. N. *J. Chem. Soc., Perkin Trans. 2* **1975**, 15–18.
108. Amendola, V.; Bergamaschi, G.; Boiocchi, M.; Fabbri, L.; Milani, M. *Chem.—Eur. J.* **2010**, *16*, 4368–4380.